COMBINED CHANNEL OF A LIDAR COMPLEX DESIGNED FOR MEASURING THE VERTICAL PROFILES OF TEMPERATURE AND AEROSOL

S.N. Volkov, B.V. Kaul', A.L. Kuznetsov, V.A. Shapranov, and D.I. Shelefontyuk

Institute of Atmospheric Optics,
Siberian Branch of the Russian Academy of Sciences, Tomsk
Received November 19, 1992

Block diagram and basic specifications of a measurement channel of a multichannel lidar complex with the primary mirror of a receiving telescope 2.2 m *in diameter are described. The temperature and aerosol measurements harness pure rotational Raman scattering by atmospheric gases and elastic scattering on the atmospheric aerosols and molecules. A technique for extracting the information about the profiles of temperature and aerosol–to–molecular scattering ratio is described.*

INTRODUCTION

Multipurpose lidar of a High–Altitude Laser Sensing Station developed at the Institute of Atmospheric Optics of the Siberian Branch of the Russian Academy of Sciences and equipped with a primary mirror of receiving antenna 2.2 m in diameter[1] makes it possible to extend the altitude range of laser radar techniques for studying the atmosphere. Among the parameters to be measured with the lidar are the vertical profiles of air temperature and moisture content that govern the condensation processes in the atmosphere. A lidar technique based on Raman light scattering[2,3] seems to be quite suitable for making such measurements. Use of differential absorption techniques, being developed at the IAO over a period of years, is also possible. In practice the use of Raman lidar techniques is complicated by small cross sections of the Raman scattering process while differential absorption techniques call for laser radiation of quite certain quality that is normally achieved at the expense of output energy. In this connection it could be advantageous to use a large receiving mirror which enables us to obtain the energy potential sufficient for measurements within the 1.5–15 km altitude range at a moderate output power of a lidar transmitter. These parameters in the surface layer must be measured with the other lidar systems since this altitude range is essentially within the shadow zone of the large lidar.[1] Depending on the ratio of a sounding beam divergence to the lidar field of view, the lidar shadow zone, in which the proportionality of a lidar return to the reciprocal square of the distance breaks down, extends to 10–20 km. However, possible uncertainty in lidar geometric function is no barrier to the application of the laser radar techniques based on measurements of ratios of return signals simultaneously at two or more frequencies, provided that optical propagation paths are identical. Below we describe an arrangement of a combined lidar measurement channel, which uses Raman and elastic light scattering simultaneously. Lidar sensing data that demonstrate the existing capabilities and potential of the lidar channel are also presented in this paper. At present the channel is equipped with a laser delivering from 0.5 to 0.8 W of mean power. For this reason we consider this channel as an intermediate operating model which enables us to develop the measurement procedure before a more favorable financial situation will make it possible to equip the channel with a transmitter delivering from 15 to 20 W of mean power in accordance with the lidar station design project.

ARRANGEMENT OF THE CHANNEL

Block diagram of the channel is depicted in Fig. 1. The beam consisting of the biharmonic of the Nd:YAG laser *1* (λ = 532 nm, 50–80 mJ energy per pulse, and 10 Hz repetition frequency) is collimated to produce a beam with angular divergence of 1 min of arc which is directed into the atmosphere by the system of three mirrors *2* exactly along the optical axis of the receiving mirror *3* with diameter of 2.2 m and focal length of 10 m.

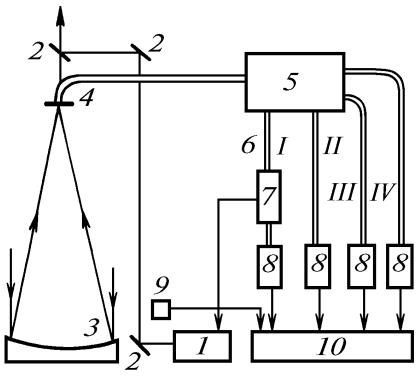

FIG. 1. Block diagram of the measurement channel. 1) laser and beam collimator, 2) beam folding mirrors, 3) parabolic primary mirror of the receiving antenna, 4) monofiber waveguide bunch, 5) double grating monochromator, 6) monofiber waveguide bunch, 7) electromechanical shutter, 8) photodetectors of subchannels I–IV, 9) photodetector triggering the recording system, and 10) recording system based on the Elektronika–60 computer.

Raman and on–wavelength radiation scattered from the atmosphere is focused by the primary mirror onto the end of the optical waveguide bunch *4* made of fused silica monofibers and is transmitted to an entrance slit of the double grating monochromator *5*. In the focal plane of the first monochromator objective two spectral sections are selected centered at frequencies coinciding with that of nitrogen pure rotational Raman lines with $J = 6$ and $J = 14$, respectively, where J is the rotational quantum number. In the same way we select the spectral section of on–wavelength light scattering. This radiation is

0235-6880/93/05 326-03 $02.00

transported by the waveguide bunch *6* to the photodetector *8* of subchannel I. The electromechanical chopper *7* is inserted in front of the photodetector to chop off the scattered radiation coming from the altitudes below 15–20 km. An electromagnetic head of the chopper generated electric pulses which after scaling down are used as synchronization pulses to actuate the laser shutter at a frequency of 10 Hz.

Extraneous light scattered by the optical parts of the first monochromator introduces the on–wavelength background. The intensity of this background is about 10^{-4} of the input one. The main portion of this extraneous background is concentrated by the second monochromator within a small region in the focal plane of the second monochromator objective. The intensity of this background radiation is comparable to that of pure rotational Raman lines of N_2 molecules. This background radiation is transmitted to the photodetector *9* of subchannel II through the bunch of monofiber waveguides. Subchannel II is intended to determine excess of aerosol light scattering over the molecular one at the altitudes the signal from which is chopped off by the chopper in subchannel I.

Radiation of two sections of pure rotational Raman spectrum of N_2 and O_2 molecules is transported by two monofiber waveguide bunches to the photodetectors of subchannels III and IV. The suppression of the on–wavelength background in these subchannels is about 10^{-8} of its intensity. For photodetectors we used photomultipliers FÉU–104 preselected to provide the necessary quality of photocounting. Photocounts from all subchannels are recorded by a four–channel photon counter built in the Élektronika–60 computer. Count rate is equal to 25 MHz.

MEASUREMENT TECHNIQUE

An example of all four signals from the subchannels of the Raman channel of High–Altitude Lidar Station is shown in Fig. 2. Each signal is described by a lidar equation

$$N_i(h)\,h^2 = A_i\,G_i(h)\,\beta_i(h)\,\exp\left\{-2\int_0^h s(h')\mathrm{d}h'\right\}\,, \qquad (1)$$

where $i = 1$, 2, 3, and 4, N_i is the number of recorded photons coming from the gate centered at the altitude H, A is the instrumental constant of the ith subchannel, $G_i(h)$ is the geometric function of the i th optical train including the receiving antenna, and $\beta_i(h)$ is the backscattering coefficient at the operation wavelength of the i th subchannel.

The quantities entering into the system of equations (1) are related to each other as follows:

$$\beta_1 = \beta_2 = \beta_a + \beta_m\,, \qquad (2)$$

$$\beta_3 + \beta_4 = k\,\beta_m\,, \qquad (3)$$

where β_a and β_m are the on–wavelength aerosol and molecular components of backscattering coefficient, k is the proportionality factor,

$$G_1(h) = F(h)\,G(h)\,, \quad G_2(h) = G_3(h) = G_4(h) = G(h)\,, \qquad (4)$$

$G(h)$ is the geometric function of the lidar optical receiving antenna, and $F(h)$ is the geometric function of the electromechanical shutter varying from 0 to 1. Because of relatively small frequency shifts of pure rotational Raman lines of N_2 and O_2 molecules, the extinction coefficient $\sigma(h)$ is assumed to be identical for all the four subchannels.

It can be easily shown that from relations (1)–(4) it follows that

$$N_1(h)/N_2(h) = F(h)A_1/A_2\,, \qquad (5)$$

$$R(h) = \kappa N_2(h)/(A_2N_3(h)/A_3 + A_2N_4(h)/A_4)\,, \qquad (6)$$

where $R(h) = [\beta_a(h) + \beta_m(h)]/\beta_m(h)$ is the so–called scattering ratio.

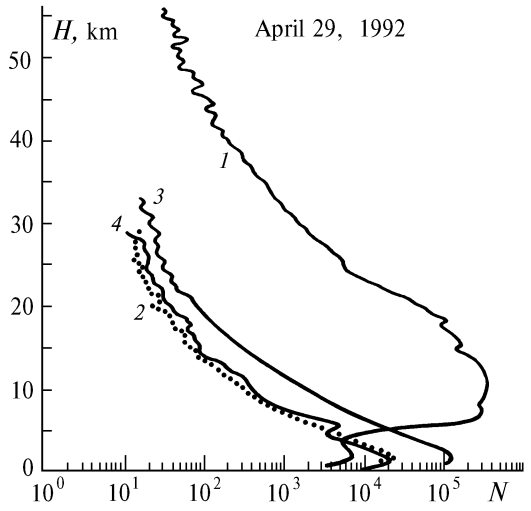

FIG. 2. Lidar returns recorded in subchannels I–IV (curves 1–4, respectively). N is the number of photocounts per range resolved gate ΔH = 480 m averaged over 10^4 laser shots.

The values $N_i(h)$ are measured during the course of sounding. The ratios A_i/A_j are determined by the corresponding calibration as the ratios of the subchannel photodetector responses to equal light fluxes. The coefficient k is averaged over a set of calibration measurement data in which the ratio $R(h)$ may be set *a priori*.

Thus relations (5) and (6) enable one to determine the geometric function of the mechanical shutter $F(h)$ and as a consequence, the scattering ratio within the uncertainty zone of the geometric function of the lidar antenna. In addition, the sum of lidar returns in the third and fourth subchannels allows sufficiently accurate estimation of this function by calculating the Raman lidar returns from the lower atmospheric layers using the altitude behavior of the molecular atmospheric density and the values of Raman lidar returns at altitudes of from 15 to 20 km (where the return signal is proportional to h^{-2}) as calibration data.

The temperature profile of the atmosphere is reconstructed from the ratio of return signals in subchannels III and IV. According to the technique described in Ref. 4, the profile $L(h)$ is related to the temperature profile as follows:

$$L(h) = [N_3(h) - n_3] \,/\, [N_4(h) - n_4] = \exp\,[\alpha/T(h) + b], \qquad (7)$$

where $N_3(h)$ and $N_4(h)$ are lidar returns in subchannels III and IV, in photocounts; n_3 and n_4 are the products of the mean dark current count rates by the gate duration and

number of laser shots; and, α and b are the instrumental constants depending on the choice of two sections of the pure rotational Raman spectrum of N_2 and O_2 molecules.

The absolute error in temperature measurements can be estimated by the formula

$$\delta T = T^2 \delta L/(\alpha L) , \qquad (8)$$

where δT and δL are the standard deviations of the corresponding quantities.

If we assume that the signal and background counts obey the Poisson statistics, we can write down formula (8) in the following form:

$$\delta T = T^2 \sqrt{N_3 + n_3 + L^2(N_4 + n_4)}/\alpha(N_3 - n_3) .$$

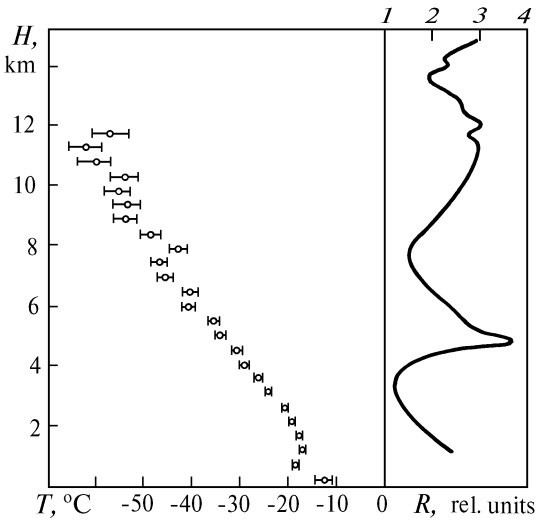

FIG. 3. The profiles of the temperature T and scattering ratio R obtained from lidar data shown by curves 2, 3, and 4 in Fig. 2.

The calibration constant α is about $7 \cdot 10^2$ K. Therefore, in order to achieve a one–degree accuracy of temperature measurements one needs to integrate up to 10^5 photocounts per gate. Temperature profile shown in Fig. 3 clearly indicates the effect of insufficient statistics of photocounts on the accuracy of temperature measurements. This effect intensifies with altitude. In view of the fact that certain investigations call for the data on temperature and moisture content in the altitude range of cirrus cloud formation, we shall have to increase substantially the energy potential of the lidar. Even a simple interpolation shows that an order of magnitude increase of the potential is needed for reaching the accuracy of temperature measurements of 1–1.5 K at the tropopause altitudes.

We are planning to undertake certain measures for improving the quality of optical train of the channel, but the main factor of the energy potential increase is the use of a laser delivering from 5 to 10 W of mean power. Such a laser source will contribute to the moisture content profiling and correct separation of the molecular and aerosol components of light scattering. The latter will be possible at altitudes up to 25–30 km and, as a result, the use of the well–known technique for temperature profiling[5] at high altitudes from the intensity of Rayleigh scattering will be allowed.

REFERENCES

1. B.V. Kaul', Atmos. Oceanic Opt. **5**, No. 4, 277 (1992).
2. A. Cohen, J.A. Cooney, and K.N. Geller, Appl. Opt. **15**, No. 11, 2896 (1976).
3. Yu.F. Arshinov, S.M. Bobrovnikov, V.E. Zuev, and V.M. Mitev, Appl. Opt. **22**, No. 19, 2984 (1983).
4. S.N. Volkov, B.V. Kaul', V.A. Shapranov, and D.I. Shelefontyuk, Atmos. Oceanic Opt. **5**, No. 6, 384 (1992).
5. G.S. Kent and R.W.H. Wright, J. Atm. Terr. Phys. **32**, 917 (1969).